analytical chemistry

Article

pubs.acs.org/ac

# Indirect Nanoplasmonic Sensing Platform for Monitoring Temperature-Dependent Protein Adsorption

Joshua A. Jackman,[†] Abdul Rahim Ferhan,[†] Bo Kyeong Yoon,[†] Jae Hyeon Park,[†] Vladimir P. Zhdanov,[†,§] and Nam-Joon Cho*[,†,‡]

[†]School of Materials Science and Engineering and Centre for Biomimetic Sensor Science, Nanyang Technological University, 50 Nanyang Drive, 637553, Singapore

[‡]School of Chemical and Biomedical Engineering, Nanyang Technological University, 62 Nanyang Drive, 637459, Singapore

[§]Boreskov Institute of Catalysis, Russian Academy of Sciences, Novosibirsk 630090, Russia

Supporting Information

**ABSTRACT:** The development of highly surface-sensitive measurement approaches to monitor protein adsorption across different temperatures would advance understanding of how thermally activated processes contribute to the denaturation of adsorbed proteins. Herein, we established an indirect nanoplasmonic sensing approach to monitor the temperature-dependent adsorption and denaturation of bovine serum albumin (BSA) protein onto a silica-coated array of plasmonic gold nanodisks. A theoretical model was developed to explain how the denaturation of an individual, adsorbed protein molecule influences the localized surface plasmon resonance (LSPR) measurement response and provided an analytical framework to estimate the effect of temperature-dependent protein denaturation on the corresponding adsorption kinetics. The sensing performance of this measurement platform was also characterized across the tested range of temperatures. With increasing temperature (up to 50 °C), it was observed that adsorbed proteins undergo greater denaturation. Circular dichroism spectroscopy and dynamic light scattering experiments verified that individual BSA monomers in bulk solution had increasingly lower conformational stability at higher temperatures within this range, which correlated with the extent of denaturation in the adsorbed state. At higher temperatures, distinct kinetic profiles arising from multilayer/aggregate formation on the sensor surface were also detected. Taken together, our findings identify that the high surface sensitivity and temperature stability of LSPR sensors make them broadly useful analytical tools for monitoring thermally activated biomacromolecular interaction processes.

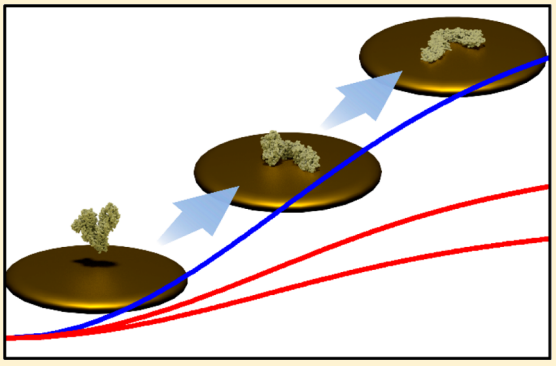

Protein adsorption at solid−liquid interfaces is widely studied because it generates knowledge about protein structure and function and is relevant to numerous applications such as materials biocompatibility (e.g., surface fouling by adsorbed proteins) and food processing (e.g., surface contamination and promoting biofilm formation).[1−3] Within this scope, one particularly important topic involves understanding how thermal unfolding of proteins influences protein adsorption and such insights provide information about the thermodynamics of protein adsorption and surface-induced denaturation. In general, it is appreciated that proteins in bulk solution undergo reversible and/or irreversible conformational changes above certain temperatures, which typically increase the amount of adsorbed protein as well as the adsorption rate.[3] Experimentally, protein adsorption at high temperatures is often measured under equilibrium conditions by reflectometry methods[4] or by determination of the residual protein concentration in bulk solution when using particulate systems.[5] While these methods provide information about the amount of bound protein and its structural configuration, it is also desirable to measure the corresponding adsorption kinetics. Spectroscopic ellipsometry has been utilized in this context,[6,7] although the technique's potential to detect conformational changes is limited[8] and requires knowing the protein refractive index increment value, which varies depending on the protein's size, amino acid composition, and conformation.[9] Similarly, the quartz crystal microbalance-dissipation (QCM-D) technique has been utilized to study protein adsorption at moderately high temperatures (up to ∼40 °C), but data interpretation is challenging due to the dependence of input parameters on temperature.[10] In some cases, electrochemical methods to monitor protein adsorption have also been utilized on suitable surfaces (e.g., platinum).[11] A broadly useful experimental approach to monitor protein adsorption across a range of temperatures is still needed, especially one that is sensitive to the conformation of adsorbed proteins.

**Received:** September 25, 2017
**Accepted:** November 6, 2017
**Published:** November 7, 2017






DOI: 10.1021/acs.analchem.7b03921
Anal. Chem. 2017, 89, 12976−12983

In this regard, nanoplasmonic sensors based on the localized surface plasmon resonance (LSPR) phenomenon are a promising surface-sensitive measurement approach to investigate protein adsorption across a wide range of temperatures.[12] LSPR generation occurs when incident light interacts with discrete metallic nanoparticles and induces the collective oscillation of free electrons in the conduction band, which in turn amplifies the electromagnetic field near the nanoparticle's surface and results in a maximum intensity of optical extinction at the plasmon resonance frequency or the corresponding wavelength ($\lambda_{max}$).[13,14] The value of $\lambda_{max}$ is highly sensitive to the local dielectric environment, and protein adsorption onto the sensor surface causes a positive $\Delta\lambda_{max}$ shift because organic molecules typically have a higher refractive index than aqueous solution.[15,16] Importantly, as the decay length of the electromagnetic field enhancement is short (5−20 nm) and comparable to the length scale of proteins, LSPR-based nanoplasmonic sensors are also sensitive to the conformation of adsorbed proteins.[17,18]

Depending on the application, it is possible to measure protein adsorption on plasmonic nanoparticles in bulk solution[19] or onto arrays of nanoparticles on a solid support.[20] The latter approach is particularly useful for quantitative evaluation of protein adsorption and is compatible with a variety of experimental configurations. Protein adsorption onto metal nanoparticles can be directly measured, or a thin layer of a dielectric material can be deposited on top of the sensor surface in order to study protein adsorption onto dielectric coatings, in which case the underlying nanoparticles serve as indirect nanoplasmonic transducers.[21−24] In such sensors, the substrate surface is corrugated on a length scale that is comparable to the nanoparticle size. In a few cases, topographically flat nanoplasmonic substrates based on embedding the nanoparticle transducers in a dielectric matrix have also been reported.[25,26] In order to monitor $\Delta\lambda_{max}$ shifts, the optical extinction spectrum is typically acquired by ultraviolet−visible spectroscopic measurements in transmission mode, and the measurement readout is ensemble-averaged across a large number of nanoparticles within the spot of incident light. Compared to conventional optical sensor techniques (e.g., SPR, ellipsometry, reflectometry), LSPR-based nanoplasmonic sensors are technically simple to operate and have smaller probing volumes that confer lower sensitivity to bulk refractive index changes such as minor temperature variations.[27] The latter feature would be particularly advantageous for monitoring protein adsorption at different temperatures. Such experiments have not yet been attempted although there are a few LSPR reports describing the effect of temperature on glucose detection in serum samples,[28] the optical response of polymer-functionalized gold nanoprisms,[29] vesicle adsorption and deformation,[30] and heterogeneous catalytic reactions.[31]

Herein, the main objective was to investigate the temperature-dependent adsorption of bovine serum albumin (BSA) protein onto silica-coated gold nanodisk arrays by indirect nanoplasmonic sensing measurements, thereby establishing an analytical framework to interpret LSPR measurement data collected in protein adsorption studies. BSA is a 66 kDa protein that was selected for the experimental work because it is widely studied as a model of serum albumins and utilized in various biochemical applications.[32] The range of experimental temperatures was incrementally varied between 25 and 70 °C in order to systematically investigate how temperature influences protein adsorption with respect to changing solution properties (e.g., viscosity) as well as inducing conformational changes in protein structure in the bulk solution. Within this scope, we sought to explore the particularly unique advantages of indirect nanoplasmonic sensing measurements for tracking protein adsorption and denaturation (see ref 3 and references therein) and chose silica as the model substrate because it is a widely used hydrophilic surface to study protein adsorption in general (concerning the hydrophilicity of this surface, see, e.g., ref 33) and also a popular dielectric material for coating gold-based nanoplasmonic sensors.[34] Of particular relevance to the present study, BSA is known to be a "soft" protein that undergoes substrate-induced conformational changes upon adsorption,[35−38] resulting in denaturation (unfolding) that is expected to influence the net spatial proximity of amino acids to the sensor surface and hence the LSPR measurement response. Such measurement capabilities would be useful for improving our knowledge of how temperature affects BSA adsorption, especially on silica for which there has only been one previous report[39] that focused on the residence time of individual protein molecules at low surface coverage.

Indeed, from a broader perspective, while a large number of experimental studies have investigated the effect of temperature on BSA adsorption on various surfaces and shown that the adsorption rate generally increases with temperature,[40−46] understanding the interplay of temperature-dependent effects on protein structure in solution, the adsorption rate, and denaturation of adsorbed protein remains to be clarified. This question is particularly significant to consider in the range of moderately high temperatures (30−60 °C) where BSA molecules undergo reversible conformational changes in the bulk solution,[47] and correlating this thermal behavior in solution with BSA protein adsorption and substrate-induced denaturation is an outstanding goal. To address this question, we build on previous efforts to understand the LSPR-related physics behind the adsorption of biological nanoparticles (vesicles)[48−50] and analyze how substrate-induced denaturation would influence the LSPR measurement response for an individual, adsorbed protein molecule. This theoretical analysis provides the basis for interpreting the LSPR experimental data.

## MATERIALS AND METHODS

**Circular Dichroism (CD) Spectroscopy.** The secondary structure of 25 $\mu$M BSA at different temperatures was investigated by temperature-controlled CD spectroscopy. The helicity ($f_H$) of BSA protein was calculated on the basis of the change of molar ellipticity at 222 nm, $[\theta]_{222}$, based on the following equation:[51]

$$f_H = ([\theta]_{222} - 3000)/(-36000 - 3000)$$

More details are provided in the Supporting Information.

**LSPR Measurement Operation.** An Insplorion XNano instrument (Insplorion AB, Gothenburg, Sweden) was employed to perform ensemble-averaged LSPR measurements on silica-coated gold nanodisk arrays in optical transmission mode, as previously described.[48] The recorded spectra were analyzed using the Insplorer software (Insplorion AB) across the 450 to 900 nm region of the extinction spectrum, and the centroid (peak) position in the extinction spectrum was determined by high-order polynomial fitting.[52] More details are provided in the Supporting Information.

**Physical Background of the LSPR Response.** We define $\Delta\lambda_{max}$ as the adsorption-related wavelength shift at the



DOI: 10.1021/acs.analchem.7b03921
Anal. Chem. 2017, 89, 12976−12983

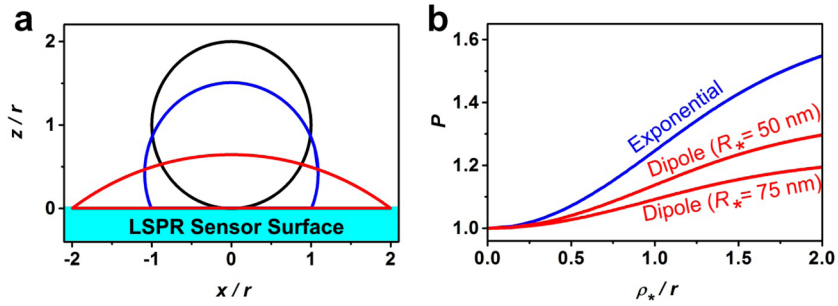


**Figure 1.** Theoretically calculated effect of protein deformation on LSPR measurement response. (a) Shapes of an adsorbed protein. In solution, the protein is assumed to be spherical with radius $r$. The adsorbed protein is represented as a nondeformed sphere (black) or a truncated sphere with $\rho_* = r$ (blue) or $\rho_* = 2r$ (red). (b) Normalized LSPR response as a function of the radius of the protein−substrate contact area (normalized to $r$). The blue and red lines correspond to exponential and power-law (dipole) evanescent field descriptions [eqs 2 and 3], respectively.

temperature of measurement and show here theoretically how protein denaturation can influence $\Delta\lambda_{max}$. The analysis is focused on protein adsorption limited to one layer, and the model predictions are intended to provide a theoretical basis for interpreting the experimental data in applicable cases. In analogy with conventional SPR spectroscopy,[53] the LSPR wavelength shift measured during protein adsorption can be represented as

$$\Delta\lambda_{max} \propto CF \tag{1}$$

where $C$ is the protein surface concentration and $F$ is the function describing the contribution of a single protein molecule to the signal. Extending this analogy to the calculation of $F$ (see, e.g., refs 13, 14, and 54), one has

$$F = \int_0^h \pi\rho^2(z)\exp(-2z/l_d)dz \tag{2}$$

where $z$ is the coordinate perpendicular to the sensor surface ($z = 0$ corresponds to this surface), $h$ is the protein size in this direction, $\pi\rho^2(z)dz$ is an element of the protein volume (the protein cross-section along the sensor surface and is assumed to be circular; $\rho(z)$ is the corresponding radius), and $l_d$ is the decay length of the evanescent electromagnetic field (the LSPR experiments with films[55] indicate that $l_d/2 \cong 5$ nm). Concerning eq 2, one should bear in mind that, in the case of conventional SPR spectroscopy, the exponential weight, $\exp(-2z/l_d)$, in the expression for the measurement signal is validated by the general equations describing the light propagation (in particular, $l_d$ can be expressed via the optical constants), while for LSPR this is just the simplest function used for fitting (see, e.g., numerical calculations[55]).

Physically, a more reasonable approach[48] is based on the dipole approximation for describing the electromagnetic field around plasmonic nanoparticles. The corresponding equations are well-known to be exact in the case of spherical nanoparticles. For the LSPR case, the use of the dipole approximation was validated by the fact that, by analogy with spherical nanoparticles, the field around plasmonic nanodisks is dominated by the dipole term. Following this line, one can replace the exponential function employed in eq 2 by $1/(R_* + z)^6$, where $R_*$ is the effective radius corresponding to the regions making the main contribution to the LSPR signal ($R_*$ is comparable to the average length scale of a metal nanoparticle) or, more specifically, to the corrugated surface regions near the plasmonic nanoparticles. The contribution of the adsorbate located on the flat surface regions not contacting the plasmonic nanoparticles can be neglected. Then, eq 2 can be rewritten as

$$F = \int_0^h \frac{\pi\rho^2(z)dz}{(R_* + z)^6} \tag{3}$$

According to this equation, the length scale of the region contributing to $F$ is $\Delta z \cong R_*/5$. Concerning the factor $1/(R_* + z)^6$ used in the equation, we may add that, in ref 48, it was partly validated by referring to the results obtained in ref 56 where LSPR sensors were not discussed explicitly. In the context of LSPR sensors, the factor $1/(R_* + z)^6$ was employed, e.g., in the first part of ref 57 assuming $z \ll R$ and replacing $1/(R_* + z)^6$ by $1/R_*^6$ [with this approximation, the authors obtained their eq (6)].

To show the effect of denaturation of adsorbed proteins on the LSPR signal, we consider that a protein is shaped approximately as a sphere of radius $r$ in the nondeformed state and a truncated sphere in the deformed state when denaturation occurs (Figure 1a). For the model calculations, we assume that the protein volume is conserved across the nondeformed and deformed states. For a truncated sphere of radius $r_*$, this condition yields

$$\frac{4\pi r_*^3}{3} - \pi r_* \chi^2 + \frac{\pi\chi^3}{3} = \frac{4\pi r^3}{3} \tag{4}$$

where $\chi$ is the height of the truncated region. In this case, the radius of the protein−substrate contact area is given by $\rho_* = [r_*^2 - (r_* - \chi)^2]^{1/2}$.

Using eq 4, $r_*$ can be expressed as a function of $r$ and $\chi$ (or $\rho_*$), and $F$ can then be calculated for the cases with and without deformation of an adsorbed protein. The ratio of the corresponding values, designated as $P$, is a measure of the effect of protein denaturation on $\Delta\lambda_{max}$ at the level of a single protein. For a given protein surface concentration, $P$ can be identified with the ratio $\Delta\lambda_{max}/\Delta\lambda^o_{max}$ where $\Delta\lambda^o_{max}$ is the response corresponding to adsorbed, nondeformed protein molecules.

Using BSA as an example, we consider that the shape of a nondeformed protein is spherical with $r = 3$ nm. To describe the power-law evanescent field [eq 3], we use $R_* = 75$ nm (this value was validated in ref 49) or $R_* = 50$ nm (for comparison). In this case, the shape of a deformed protein is determined by the dimensionless ratio $\rho_*/r$, and accordingly, $P$ depends on $\rho_*/r$ and also on the dimensionless ratio $r/R_* = 3/75 = 0.04$ (Figure 1b, red lines). For the exponential evanescent field of eq 2, $P$ depends on $\rho_*/r$ and also on the dimensionless ratio $2r/l_d$. Employing $r = 3$ nm and $l_d/2 \cong 5$ nm (cf. ref 54), we have $2r/l_d \cong 0.6$. The latter value was used in calculations (Figure 1b, blue line).



DOI: 10.1021/acs.analchem.7b03921
Anal. Chem. 2017, 89, 12976−12983

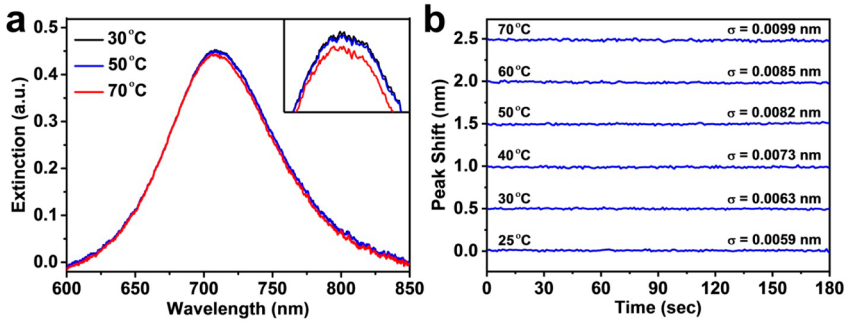


**Figure 2.** Evaluation of nanoplasmonic sensor performance in aqueous environments at different temperatures. (a) Characteristic extinction spectrum of a silica-coated gold nanodisk array in an aqueous environment at different experimental temperatures: 30 °C (black); 50 °C (blue); 70 °C (red). Inset shows the magnified view of the extinction maximum. (b) Comparison of spectral noise at different experimental temperatures. The noise level is defined as the standard deviation of repeated measurements on a blank sample over a 3 min time period.

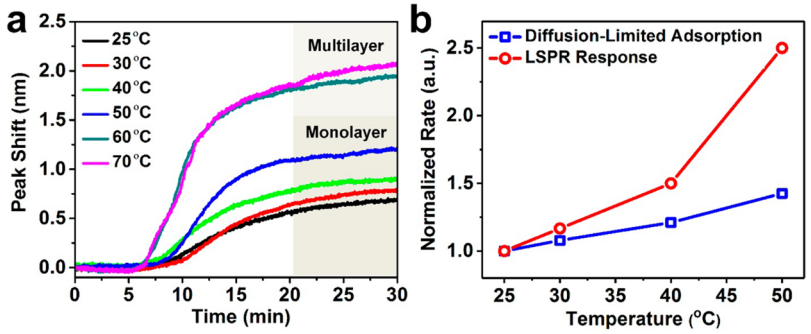


**Figure 3.** LSPR measurements of temperature-dependent BSA protein adsorption onto silicon oxide. (a) LSPR peak shift as a function of time for 100 $\mu$M BSA adsorption onto silica-coated gold nanodisk arrays. A measurement baseline was first established, and then, protein was injected under continuous flow conditions starting at $t$ = 5 min. (b) Comparison of the normalized maximum rate of change in the LSPR signal arising from BSA protein adsorption and deformation ($\partial\Delta\lambda_{max}/\partial t$) based on data from panel (a) and the normalized rate of diffusion-limited adsorption alone calculated according to eq 6 for the experimental conditions at different temperatures (see Supporting Information). The rates are normalized on the basis of the values obtained for the 25 °C case.

The two sets of model predictions, based on the different descriptions of the evanescent field decay, show similar trends. Quantitatively, the effect predicted is stronger for the exponential field, because it drops faster with increasing $z$. With increasing denaturation of a single protein, its contribution to the LSPR signal increases because, on average, the protein's molecular density is expected to be closer to the sensor surface. As protein denaturation is an activated process,[58] the extent of denaturation for an adsorbed protein is greater at higher temperatures. In this context, it should be emphasized that the model predictions are based on the assumption that protein volume is conserved. This assumption leads to a minimum estimate of the deformation effect. For soft proteins like BSA, protein volume is usually not exactly conserved[59] and surface-induced denaturation can lead to protein spreading.[60] In addition, surface-induced denaturation often involves dehydration of adsorbed protein molecules, which can increase the protein's refractive index increment value.[61] Both additional factors would further increase the effect of protein denaturation on the LSPR signal for an adsorbed protein molecule.

In summary, the theoretical model shows that the denaturation of an adsorbed protein molecule on the sensor surface causes an increase in the corresponding $\Delta\lambda_{max}$ shift. In the Supporting Information, our theoretical analysis is further extended to estimate how temperature affects the rate of protein adsorption and to provide an analytical framework to estimate the effect of temperature-dependent protein denaturation on the corresponding adsorption kinetics. We also provide additional justification to support our theoretical approach.

## RESULTS AND DISCUSSION

The LSPR measurement platform consists of well-separated, noninteracting gold nanodisks that were fabricated on a glass substrate by hole-mask colloidal lithography,[62] and the entire substrate was then sputter-coated with a thin (~10 nm) layer of silicon dioxide afterward. The sensor substrates were next assembled in a temperature-controlled microfluidic chamber, and the experiments were conducted in a flow-through configuration, with the flow rate controlled by a peristaltic pump. For the LSPR measurements, the optical extinction spectra were collected in transmission mode and the specific $\lambda_{max}$ position was determined by the centroid method of analysis. The $\lambda_{max}$ position was around 711 nm in aqueous buffer solution (10 mM Tris [pH 7.5] with 150 mM NaCl) at ambient room temperature (25 °C), and a slight decrease in the $\lambda_{max}$ position was observed with increasing temperature. In the representative spectra collected at 30, 50, and 70 °C, the $\lambda_{max}$ position decreases from 711.6 to 710.8 nm upon heating from 30 to 70 °C (Figure 2a). This $\lambda_{max}$ shift is attributed to the temperature-related decrease of the refractive index ($n$) of the bulk solution,[63] which corresponds to $\Delta n$ = −0.007 RIU. As the bulk refractive index sensitivity of the silicon oxide-coated gold nanodisks used in these experiments is 100 nm/RIU, the theoretical $\Delta\lambda_{max}$ shift is 100 nm/RIU × −0.007 RIU = −0.7 nm, which agrees well with the measurement result. It also


DOI: 10.1021/acs.analchem.7b03921
Anal. Chem. 2017, 89, 12976−12983

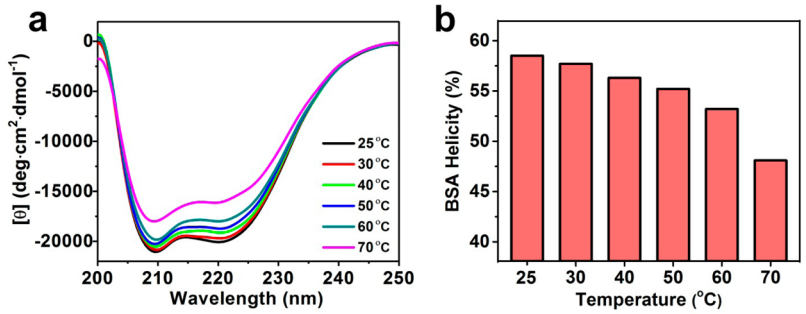


**Figure 4.** Effect of temperature on BSA protein secondary structure in solution. (a) Circular dichroism spectra of BSA protein in solution at different temperatures and expressed as mean residue ellipciticity [$\theta$]. (b) Fractional helicity of BSA protein in solution based on measured [$\theta$] values at 222 nm.

supports that the effect of temperature on the plasmonic properties of the gold nanodisks themselves (due to the Au-lattice expansion) is less important.[64,65]

While the LSPR spectral signature is known to be only weakly sensitive to the experimental temperature,[64] the dependence of the spectral noise on temperature is not widely reported for measurement operation in liquid environments. Therefore, we estimated the spectral noise by determining the standard deviation ($\sigma$) of the $\lambda_{max}$ position over 3 min for the nanodisk array immersed in aqueous buffer solution. In the present experiments, 300 spectral frames with an integration time of 3 ms per frame were collected for each averaged data point, representing a temporal resolution of 0.9 s and hence the spectral noise was determined over a total of 200 data points. As presented in Figure 2b, there was a moderate increase in $\sigma$ from $5.9 \times 10^{-3}$ to $9.9 \times 10^{-3}$ nm as the temperature rose from 25 to 70 °C. On the basis of the bulk refractive index sensitivity of 100 nm/RIU, this noise translates into a minimum refractive index resolution of between $5.9 \times 10^{-5}$ and $9.9 \times 10^{-5}$ RIU depending on the temperature. Hence, the spectral noise and corresponding detection performance slightly decrease with increasing temperature but remain comparable.

We next investigated the effect of temperature on 100 $\mu$M BSA adsorption onto the silica-coated sensor surface (Figure 3a). The BSA samples were preincubated at the experimental temperature for 30 min before injection into the temperature-controlled measurement chamber. In all cases, monotonic adsorption until saturation was observed, yielding characteristic $\Delta\lambda_{max}$ shifts. At 25 °C, the final $\Delta\lambda_{max}$ shift was 0.6 nm. With increasing temperature, a slight increase in the $\Delta\lambda_{max}$ shift was observed up to 40 °C, with recorded $\Delta\lambda_{max}$ shifts of 0.7 and 0.8 nm at 30 and 40 °C, respectively. A more appreciable yet still moderate increase in the final $\Delta\lambda_{max}$ shift to 1.1 nm was observed at 50 °C. In contrast, at 60 °C, BSA adsorption led to a final $\Delta\lambda_{max}$ shift of 1.8 nm, and the shift further increased to 2.1 nm at 70 °C. This abrupt increase in the final $\Delta\lambda_{max}$ shift along with the difference in kinetic profiles is consistent with a change in the adsorption pathway from a protein monolayer at lower temperatures[4] (≤50 °C) to protein aggregates and/or a multilayer at higher temperatures[5] (≥60 °C). There was also a distinct dependence of the final $\Delta\lambda_{max}$ shift on temperature for protein monolayers, suggesting that temperature influences not only the adsorption rate but also the extent of substrate-induced conformational changes (i.e., deformation) of adsorbed protein and its surface concentration at saturation.

To understand how deformation of adsorbed proteins influences the LSPR measurement response, we focused on the temperature range of 25 to 50 °C wherein protein monolayers form and scrutinized the experimentally measured rate of change in the LSPR signal during the initial stage of protein adsorption. In this stage, the surface coverage of adsorbed proteins is low and the rate of change in the LSPR signal is nearly constant because the adsorption rate is controlled by the bulk diffusion of BSA monomers in solution.[66] This allowed us to determine the rate of change in the LSPR signal (expressed in nm/min units) by calculating time derivative plots from the data presented in Figure 3a and identifying the maximum rate of change in the LSPR signal as a function of temperature.[67] At 25 °C, the rate was 0.06 nm/min and increased to 0.07, 0.09, and 0.15 nm/min at 30, 40, and 50 °C, respectively. Hence, on a normalized scale, the experimentally measured rate of change in the LSPR signal increased by 2.5 times from 25 to 50 °C (Figure 3b, red circles). It should be emphasized that the measured rate is affected by not only diffusion-limited adsorption but also the extent of substrate-induced protein deformation. Hence, while the diffusion-limited adsorption rate is constant when the surface coverage of adsorbed proteins is low, the magnitude of the rate will also depend on the deformation of adsorbed protein molecules. In particular, greater protein deformation would lead to increased contact with the sensor surface, in turn increasing the net $\Delta\lambda_{max}$ contribution per BSA molecule as well as the corresponding rate of change in the LSPR signal because a larger portion of the molecular mass would be in a region of higher evanescent field intensity.

To clarify the origin of the temperature-dependent increase in the measured rate, we calculated how the rate of diffusion-limited protein adsorption scales according to temperature [see eq 6 in the Supporting Information and take into account that the protein diffusion coefficient depends on the solution viscosity; for the dependence of the viscosity on temperature, see ref 68]. It is important to note that the theoretical calculations [based on eq 6 in the Supporting Information] predict only how temperature affects the rate of diffusion-limited adsorption and do not take into account the effect of temperature on substrate-induced protein deformation. As such, the trend in the experimentally observed rate (related to protein adsorption and denaturation) as a function of temperature can be compared to the trend in diffusion-limited adsorption as a function of temperature, and deviations between the two rate trends can be assigned to temperature-dependent effects on the deformation of adsorbed proteins. Following this approach, it is noted that, with increasing temperature, the diffusion-limited adsorption rate increases by 1.4 times across the temperature range of 25 to 50 °C (Figure 3b, blue squares). Hence, the experimentally measured rate of


DOI: 10.1021/acs.analchem.7b03921
Anal. Chem. 2017, 89, 12976−12983

change in the LSPR signal increased more appreciably than the predicted increase arising from the temperature-dependent rate of diffusion-limited adsorption alone. This finding supports that temperature influences the extent of deformation of adsorbed proteins on the sensor surface, namely, that there is increased deformation of adsorbed proteins at higher temperatures. In particular, the additional increase of the rate, namely, $\partial\Delta\lambda_{max}/\partial t$, is greater with increasing temperature, and its scale is comparable to that predicted by the model taking protein deformation into account and assuming that protein spreading is nearly negligible ($\rho_*/r < 0.5$) at 25 °C and appreciable ($\rho_*/r \geq 2$) at 50 °C (cf. Figure 1). This conclusion further supports that the extent of protein deformation is greater when BSA molecules have lower conformational stability in solution.

In order to corroborate the LSPR data with the conformational stability of BSA in solution, circular dichroism (CD) spectroscopic measurements were conducted on solution-phase BSA as a function of temperature (Figure 4a). As thermal denaturation of BSA occurs through a series of conformational transitions from $\alpha$-helix to $\beta$-sheet structures, followed by partial unfolding to a random coil, the degree of change in the BSA secondary structure in bulk solution can be inferred from the overall loss in fractional helicity. Indeed, the probability of stabilization of protein folding increases with greater helicity, and therefore, the fractional helicity provides an indication of conformational stability.[69] At 25 °C, the fractional helicity was calculated to be 59%, as expected for native BSA (Figure 4b). An incremental decrease down to 53% helicity was observed at 60 °C or lower, supporting that the conformational stability of BSA in solution decreases at higher temperatures within this temperature range. In contrast, there was a sharper decrease to 48% at 70 °C. The measured loss in fractional helicity agrees well with previous CD studies, which have demonstrated that heating BSA in solution at temperatures at or below 60 °C resulted in mainly reversible transformation from $\alpha$-helix to $\beta$-sheet structures, while heating above 60 °C results in irreversible loss of structure due to partial unfolding and aggregation of BSA molecules.[47,70−75]

As the molecular size of proteins affects the diffusion flux of proteins in bulk solution, dynamic light scattering (DLS) measurements were also performed in order to determine the hydrodynamic diameter of BSA molecules as a function of temperature (Figure 5). The hydrodynamic diameter of BSA monomers at room temperature was determined to be 8.2 ± 1.7 nm, which agrees well with literature reports.[75,76] When the temperature was gradually raised from room temperature to 65 °C in 5 °C intervals, there was no change in the measured size, verifying that BSA remained in the monomeric state despite significant changes in secondary structure. In marked contrast, when the temperature was further raised to 70 °C, the hydrodynamic diameter increased to 23.2 ± 5.4 nm, indicating BSA aggregation and oligomer formation. The onset of aggregation at this temperature agrees well with a previous report, which showed that an increase in hydrodynamic diameter occurred above ∼63 °C.[77] The findings are also consistent with the CD spectroscopic data and support that, up to a certain temperature, BSA proteins can undergo partial, reversible unfolding (decreased helicity) while the effective size of protein molecules in solution remains unchanged. These results establish that, in the temperature range of 25 to 50 °C, there is a correlation between partial unfolding of BSA protein in solution and the extent of protein denaturation on the silica surface.

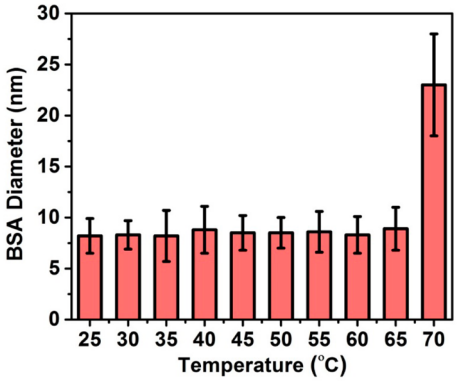


**Figure 5.** Effect of temperature on BSA protein size in solution. DLS experiments were performed on BSA protein in solution, and the temperature in the measurement chamber was controlled. The hydrodynamic diameter is represented as the mean ± standard deviation from five measurements.

To explain this observation, there are two possible ways that temperature affects the rate of change in the LSPR signal. As described above, the first way is that the denaturation of adsorbed proteins results in greater protein spreading such that the molecular density of an adsorbed protein is, on average, nearer to the sensor surface. In turn, the net $\Delta\lambda_{max}$ contribution per BSA molecule increases because a larger portion of the molecular mass is in a region of higher evanescent field intensity. Second, it is known that most BSA molecules attach weakly to silica surfaces[78] and the ensemble-averaged measurement response describes the net rate of adsorbing and desorbing BSA molecules. While the theoretical analysis [cf. eq (6) in the Supporting Information] accounts for the effect of temperature on the adsorption rate, it does not account for its effect on the desorption rate. If protein attachment at higher temperatures is stronger, then the rate of desorption would be smaller, hence contributing to a larger net rate of change in the LSPR signal. Indeed, it is known that protein adsorption becomes more irreversible with greater denaturation of bound protein.[79] The two effects of temperature, increased spreading and reduced desorption, are self-consistent, and both support that there is greater deformation of adsorbed proteins with increasing temperature, as detected by the LSPR measurements. These findings are further supported by the CD results that indicate BSA molecules in solution become partially denatured at higher temperatures. Greater denaturation of protein molecules in solution in turn decreases conformational stability, which is defined as the change in free energy between the existing conformational state and the completely unfolded state.[80] With decreasing conformational stability, an adsorbed protein will undergo a greater rate of conformational changes until reaching an optimal number of contact points between the protein molecule and silica surface.[81,82] Hence, a protein with lower conformational stability in solution will become more denatured upon adsorption, and hence, the adsorption will become more irreversible. These trends agree well with work by Karlsson et al., which described how engineered variants of human carbonic anhydrase II protein with lower conformational stability adsorb more irreversibly onto solid supports, largely independent of the support properties (negatively charged, positively charged, hydrophilic, hydrophobic).[83] Indeed, as noted above, our finding revealed a correspondence


DOI: 10.1021/acs.analchem.7b03921
Anal. Chem. 2017, 89, 12976−12983

between the extent of loss of protein helicity and the apparent rate of change in the LSPR signal.

Furthermore, the LSPR measurements indicate that the incremental, reversible thermal denaturation of BSA in solution up to 50 °C is correlated with a moderate increase in the final $\Delta\lambda_{max}$ shift at saturation as well. At saturation, the net measurement response depends on both the extent of protein denaturation/spreading and the total number of adsorbed protein molecules. Indeed, greater protein spreading correlates with a larger area occupied per molecule, which would effectively lower the total number of adsorbed molecules at saturation.[84] The observed opposed trend indicates that, in the high coverage regime, newly arriving proteins can adsorb at remaining small spots between earlier adsorbed spread proteins; i.e., the adsorbed protein molecules can be in different states at high coverage, and this becomes more favorable with increasing temperature. In this context, we may notice that the change of the BSA state (orientation) with increasing coverage was earlier implied in ref 85.

## CONCLUSION

In this work, we have presented an indirect nanoplasmonic sensing approach that is capable of tracking the adsorption and denaturation of BSA protein onto a silica-coated array of plasmonic gold nanodisks. On the basis of a theoretical model, it was shown that the LSPR measurement response for a single, adsorbed protein is expected to increase with its greater denaturation on the sensor surface. This model was applied to interpret experimental data, and it was observed that, with increasing temperature (up to 50 °C), adsorbed proteins undergo greater denaturation on account of lower conformational stability in bulk solution. These findings have important implications for the protein adsorption field as a whole. In high temperature conditions, proteins in bulk solution undergo irreversible conformational changes that cause protein oligomerization and it is known that protein adsorption is particularly high under such conditions. On the other hand, at moderate temperatures, it is less understood how reversible conformational changes in protein structure influence adsorption kinetics. By utilizing the nanoplasmonic sensing approach, it was discovered herein that the denaturation of adsorbed proteins increases with a greater extent of reversible conformational changes in the protein structure in bulk solution, and this trend can be explained by the relationship between conformational stability and the propensity to denature in the adsorbed state. To our knowledge, these findings offer the first experimental evidence directly correlating the conformational stability of a protein in bulk solution with the extent of denaturation in the adsorbed state. Looking forward, the methodology we used (LSPR in combination with bulk measurements) can be applied across a wide range of proteins in different solution conditions and opens the door to understanding how thermally activated processes contribute to the denaturation of adsorbed proteins and other classes of biomacromolecules and soft-matter nanoparticles.

## ASSOCIATED CONTENT

### Supporting Information

The Supporting Information is available free of charge on the ACS Publications website at DOI: 10.1021/acs.analchem.7b03921.

Additional details on the physical background of the LSPR response, analytical framework for LSPR data interpretation, and experimental methods (PDF)

## AUTHOR INFORMATION

### Corresponding Author

*E-mail: njcho@ntu.edu.sg.

### ORCID

Nam-Joon Cho: 0000-0002-8692-8955

### Notes

The authors declare no competing financial interest.

## ACKNOWLEDGMENTS

This work was supported by the National Research Foundation of Singapore through a Competitive Research Programme grant (NRF-CRP10-2012-07) and a Proof-of-Concept grant (NRF2015NRF-POC0001-19) as well as through the Center for Precision Biology at Nanyang Technological University. The support of the Russian Federal Agency for Scientific Organizations (project 0303-2016-0001) is also appreciated.

## REFERENCES

(1) Nakanishi, K.; Sakiyama, T.; Imamura, K. *J. Biosci. Bioeng.* **2001**, *91*, 233−244.
(2) Gray, J. J. *Curr. Opin. Struct. Biol.* **2004**, *14*, 110−115.
(3) Rabe, M.; Verdes, D.; Seeger, S. *Adv. Colloid Interface Sci.* **2011**, *162*, 87−106.
(4) Kiesel, I.; Paulus, M.; Nase, J.; Tiemeyer, S.; Sternemann, C.; Rüster, K.; Wirkert, F. J.; Mende, K.; Büning, T.; Tolan, M. *Langmuir* **2014**, *30*, 2077−2083.
(5) Fukuzaki, S.; Urano, H.; Nagata, K. *J. Ferment. Bioeng.* **1995**, *80*, 6−11.
(6) Arnebrant, T.; Barton, K.; Nylander, T. *J. Colloid Interface Sci.* **1987**, *119*, 383−390.
(7) Santos, O.; Nylander, T.; Paulsson, M.; Trägårdh, C. *J. Food Eng.* **2006**, *74*, 468−483.
(8) Elwing, H. *Biomaterials* **1998**, *19*, 397−406.
(9) Zhao, H.; Brown, P. H.; Schuck, P. *Biophys. J.* **2011**, *100*, 2309−2317.
(10) Ohlsson, G.; Tigerström, A.; Höök, F.; Kasemo, B. *Soft Matter* **2011**, *7*, 10749−10755.
(11) Cabilio, N. R.; Omanovic, S.; Roscoe, S. G. *Langmuir* **2000**, *16*, 8480−8488.
(12) Jackman, J. A.; Ferhan, A. R.; Cho, N.-J. *Chem. Soc. Rev.* **2017**, *46*, 3615−3660.
(13) Willets, K. A.; Van Duyne, R. P. *Annu. Rev. Phys. Chem.* **2007**, *58*, 267−297.
(14) Anker, J. N.; Hall, W. P.; Lyandres, O.; Shah, N. C.; Zhao, J.; Van Duyne, R. P. *Nat. Mater.* **2008**, *7*, 442−453.
(15) Dahlin, A. B.; Wittenberg, N. J.; Höök, F.; Oh, S.-H. *Nanophotonics* **2013**, *2*, 83−101.
(16) Estevez, M.-C.; Otte, M. A.; Sepulveda, B.; Lechuga, L. M. *Anal. Chim. Acta* **2014**, *806*, 55−73.
(17) Hall, W. P.; Anker, J. N.; Lin, Y.; Modica, J.; Mrksich, M.; Van Duyne, R. P. *J. Am. Chem. Soc.* **2008**, *130*, 5836−5837.
(18) Hall, W. P.; Modica, J.; Anker, J.; Lin, Y.; Mrksich, M.; Van Duyne, R. P. *Nano Lett.* **2011**, *11*, 1098−1105.
(19) Teichroeb, J.; Forrest, J.; Ngai, V.; Jones, L. *Eur. Phys. J. E: Soft Matter Biol. Phys.* **2006**, *21*, 19−24.
(20) Haes, A. J.; Van Duyne, R. P. *J. Am. Chem. Soc.* **2002**, *124*, 10596−10604.
(21) Mazzotta, F.; Johnson, T. W.; Dahlin, A. B.; Shaver, J.; Oh, S.-H.; Höök, F. *ACS Photonics* **2015**, *2*, 256−262.
(22) Frost, R.; Wadell, C.; Hellman, A.; Molander, S.; Svedhem, S.; Persson, M.; Langhammer, C. *ACS Sensors* **2016**, *1*, 798−806.



DOI: 10.1021/acs.analchem.7b03921
*Anal. Chem.* 2017, 89, 12976−12983

(23) Zen, F.; Karanikolas, V. D.; Behan, J. A.; Andersson, J.; Ciapetti, G.; Bradley, A. L.; Colavita, P. E. *Langmuir* **2017**, *33*, 4198−4206.
(24) Frost, R.; Langhammer, C.; Cedervall, T. *Nanoscale* **2017**, *9*, 3620−3628.
(25) Jose, J.; Jordan, L. R.; Johnson, T. W.; Lee, S. H.; Wittenberg, N. J.; Oh, S. H. *Adv. Funct. Mater.* **2013**, *23*, 2812−2820.
(26) Nugroho, F. A. A.; Frost, R.; Antosiewicz, T. J.; Fritzsche, J.; Larsson Langhammer, E. M.; Langhammer, C. *ACS Sensors* **2017**, *2*, 119−127.
(27) Mayer, K. M.; Hafner, J. H. *Chem. Rev.* **2011**, *111*, 3828−3857.
(28) Shen, X. W.; Huang, C. Z.; Li, Y. F. *Talanta* **2007**, *72*, 1432−1437.
(29) Joshi, G. K.; Smith, K. A.; Johnson, M. A.; Sardar, R. *J. Phys. Chem. C* **2013**, *117*, 26228−26237.
(30) Oh, E.; Jackman, J. A.; Yorulmaz, S.; Zhdanov, V. P.; Lee, H.; Cho, N.-J. *Langmuir* **2015**, *31*, 771−781.
(31) Wettergren, K.; Hellman, A.; Cavalca, F.; Zhdanov, V. P.; Langhammer, C. *Nano Lett.* **2015**, *15*, 574−580.
(32) Peters, T. *Adv. Protein Chem.* **1985**, *37*, 161−245.
(33) Bergkvist, M.; Carlsson, J.; Oscarsson, S. *J. Biomed. Mater. Res.* **2003**, *64A*, 349−356.
(34) Lindquist, N. C.; Nagpal, P.; McPeak, K. M.; Norris, D. J.; Oh, S.-H. *Rep. Prog. Phys.* **2012**, *75*, 036501.
(35) Norde, W.; Favier, J. P. *Colloids Surf.* **1992**, *64*, 87−93.
(36) Roach, P.; Farrar, D.; Perry, C. C. *J. Am. Chem. Soc.* **2005**, *127*, 8168−8173.
(37) Norde, W. *Colloids Surf., B* **2008**, *61*, 1−9.
(38) Jachimska, B.; Tokarczyk, K.; Łapczyńska, M.; Puciul-Malinowska, A.; Zapotoczny, S. *Colloids Surf., A* **2016**, *489*, 163−172.
(39) Langdon, B. B.; Kastantin, M.; Schwartz, D. K. *Biophys. J.* **2012**, *102*, 2625−2633.
(40) Kiss, É. *Colloids Surf., A* **1993**, *76*, 135−140.
(41) Sakiyama, T.; Toyomasu, T.; Nagata, A.; Imamura, K.; Nakanishi, K.; Takahashi, T.; Nagai, T. *J. Chem. Eng. Jpn.* **1998**, *31*, 208−213.
(42) Dias-Cabral, A.; Queiroz, J.; Pinto, N. *J. Chromatogr. A* **2003**, *1018*, 137−153.
(43) Kopac, T.; Bozgeyik, K.; Yener, J. *Colloids Surf., A* **2008**, *322*, 19−28.
(44) Mo, H.; Tay, K. G.; Ng, H. Y. *J. Membr. Sci.* **2008**, *315*, 28−35.
(45) Bellion, M.; Santen, L.; Mantz, H.; Hähl, H.; Quinn, A.; Nagel, A.; Gilow, C.; Weitenberg, C.; Schmitt, Y.; Jacobs, K. *J. Phys.: Condens. Matter* **2008**, *20*, 404226.
(46) Vidal, C. V.; Juan, A. O.; Muñoz, A. I. *Colloids Surf., B* **2010**, *80*, 1−11.
(47) Takeda, K.; Wada, A.; Yamamoto, K.; Moriyama, Y.; Aoki, K. *J. Protein Chem.* **1989**, *8*, 653−659.
(48) Jackman, J. A.; Zhdanov, V. P.; Cho, N.-J. *Langmuir* **2014**, *30*, 9494−9503.
(49) Jackman, J. A.; Spackova, B.; Linardy, E.; Kim, M. C.; Yoon, B. K.; Homola, J.; Cho, N.-J. *Chem. Commun.* **2016**, *52*, 76−79.
(50) Jackman, J. A.; Yorulmaz Avsar, S.; Ferhan, A. R.; Li, D.; Park, J. H.; Zhdanov, V. P.; Cho, N.-J. *Anal. Chem.* **2017**, *89*, 1102−1109.
(51) Morrisett, J. D.; David, J. S.; Pownall, H. J.; Gotto, A. M., Jr *Biochemistry* **1973**, *12*, 1290−1299.
(52) Dahlin, A. B.; Tegenfeldt, J. O.; Höök, F. *Anal. Chem.* **2006**, *78*, 4416−4423.
(53) Jung, L. S.; Campbell, C. T.; Chinowsky, T. M.; Mar, M. N.; Yee, S. S. *Langmuir* **1998**, *14*, 5636−5648.
(54) Larsson, E. M.; Edvardsson, M. E.; Langhammer, C.; Zorić, I.; Kasemo, B. *Rev. Sci. Instrum.* **2009**, *80*, 125105.
(55) Li, J.; Ye, J.; Chen, C.; Hermans, L.; Verellen, N.; Ryken, J.; Jans, H.; Van Roy, W.; Moshchalkov, V. V.; Lagae, L.; et al. *Adv. Opt. Mater.* **2015**, *3*, 176−181.
(56) Zhdanov, V. P.; Kasemo, B. *Appl. Phys. Lett.* **2004**, *84*, 1748−1749.
(57) Antosiewicz, T. J.; Apell, S. P.; Claudio, V.; Käll, M. *Opt. Express* **2012**, *20*, 524−533.
(58) Day, R.; Bennion, B. J.; Ham, S.; Daggett, V. *J. Mol. Biol.* **2002**, *322*, 189−203.
(59) Koo, J.; Czeslik, C. *Soft Matter* **2012**, *8*, 11670−11676.
(60) Su, T.; Lu, J.; Thomas, R.; Cui, Z.; Penfold, J. *J. Phys. Chem. B* **1998**, *102*, 8100−8108.
(61) Vörös, J. *Biophys. J.* **2004**, *87*, 553−561.
(62) Fredriksson, H.; Alaverdyan, Y.; Dmitriev, A.; Langhammer, C.; Sutherland, D. S.; Zäch, M.; Kasemo, B. *Adv. Mater.* **2007**, *19*, 4297−4302.
(63) Harvey, A. H.; Gallagher, J. S.; Sengers, J. L. *J. Phys. Chem. Ref. Data* **1998**, *27*, 761−774.
(64) Link, S.; El-Sayed, M. A. *J. Phys. Chem. B* **1999**, *103*, 4212−4217.
(65) Yeshchenko, O.; Bondarchuk, I.; Gurin, V.; Dmitruk, I.; Kotko, A. *Surf. Sci.* **2013**, *608*, 275−281.
(66) Hlady, V.; Reinecke, D.; Andrade, J. *J. Colloid Interface Sci.* **1986**, *111*, 555−569.
(67) Zan, G. H.; Jackman, J. A.; Kim, S. O.; Cho, N. J. *Small* **2014**, *10*, 4828−4832.
(68) Kestin, J.; Sokolov, M.; Wakeham, W. A. *J. Phys. Chem. Ref. Data* **1978**, *7*, 941−948.
(69) Atassi, M.; Singhal, R. *J. Biol. Chem.* **1970**, *245*, 5122−5128.
(70) Murayama, K.; Tomida, M. *Biochemistry* **2004**, *43*, 11526−11532.
(71) Giacomelli, C. E.; Norde, W. *J. Colloid Interface Sci.* **2001**, *233*, 234−240.
(72) Larsericsdotter, H.; Oscarsson, S.; Buijs, J. *J. Colloid Interface Sci.* **2005**, *289*, 26−35.
(73) Moriyama, Y.; Kawasaka, Y.; Takeda, K. *J. Colloid Interface Sci.* **2003**, *257*, 41−46.
(74) Moriyama, Y.; Watanabe, E.; Kobayashi, K.; Harano, H.; Inui, E.; Takeda, K. *J. Phys. Chem. B* **2008**, *112*, 16585−16589.
(75) Militello, V.; Casarino, C.; Emanuele, A.; Giostra, A.; Pullara, F.; Leone, M. *Biophys. Chem.* **2004**, *107*, 175−187.
(76) Jachimska, B.; Wasilewska, M.; Adamczyk, Z. *Langmuir* **2008**, *24*, 6866−6872.
(77) Yohannes, G.; Wiedmer, S. K.; Elomaa, M.; Jussila, M.; Aseyev, V.; Riekkola, M.-L. *Anal. Chim. Acta* **2010**, *675*, 191−198.
(78) Kwok, K.; Yeung, K.; Cheung, N. *Langmuir* **2007**, *23*, 1948−1952.
(79) van der Veen, M.; Stuart, M. C.; Norde, W. *Colloids Surf., B* **2007**, *54*, 136−142.
(80) Pace, C. N.; Scholtz, J. M. Measuring the Conformational Stability of a Protein. In *Protein Structure*; Oxford University Press: New York, 1997; Vol. *2*, pp 299−321.
(81) Pace, C. N.; Shirley, B. A.; McNutt, M.; Gajiwala, K. *FASEB J.* **1996**, *10*, 75−83.
(82) Moulin, A.; O'shea, S.; Badley, R.; Doyle, P.; Welland, M. *Langmuir* **1999**, *15*, 8776−8779.
(83) Karlsson, M.; Ekeroth, J.; Elwing, H.; Carlsson, U. *J. Biol. Chem.* **2005**, *280*, 25558−25564.
(84) Park, J. H.; Sut, T. N.; Jackman, J. A.; Ferhan, A. R.; Yoon, B. K.; Cho, N.-J. *Phys. Chem. Chem. Phys.* **2017**, *19*, 8854−8865.
(85) Kurrat, R.; Prenosil, J.; Ramsden, J. *J. Colloid Interface Sci.* **1997**, *185*, 1−8.



DOI: 10.1021/acs.analchem.7b03921
*Anal. Chem.* 2017, 89, 12976−12983